

# Directional Signatures of Structural Commitment: Testing Late-Time Isotropy in a Non-Markovian Cosmology

Stephen Atalebe, DOI: 10.5281/zenodo.18702637

February 19, 2026

## Abstract

The cosmological principle assumes statistical isotropy and homogeneity on large scales as an initial condition. Yet nonlinear structure formation does not proceed uniformly across directions inside any finite cosmic volume. If the effective expansion responds to accumulated nonlinear history, then uneven structural commitment may generate weak, late-time directional signatures without violating primordial isotropy.

The paper builds a computational pathway to test this idea. First, a two-region toy model demonstrates a baseline mechanism, anisotropy emerges transiently when collapse histories diverge, and the amplitude is regulated by the memory kernel, with longer memory horizons suppressing directional contrasts by temporal averaging. Second, the study moves to cosmological simulations, focusing on the TNG300-1 volume to calibrate the intrinsic structural dipole as a null baseline, verify that the preferred structural axis is coherent across late-time snapshots and strengthened by massive halos, and rule out a moving-box explanation via bulk-flow alignment tests. The study then measures a directional expansion response by fitting dipoles to the bulk-flow-subtracted radial velocity field, including shell tomography out to  $\sim 200 h^{-1}\text{Mpc}$ . In shell tomography, the outer shell shows a stable, structure aligned expansion dipole at the 1.1% level in the peculiar velocity frame.

Finally, cross-checking of methodology in TNG50-1 and stress-test the structural dipole estimator on SDSS DR8, where survey geometry dominates the raw dipole and requires mask-aware null tests. Overall, these experiments establish that a coherent structural mode in a finite volume naturally induces a coherent directional expansion anomaly. This work provides the simulation benchmark that any observational dipole test of non-Markovian expansion must first clear.

## 1 Purpose and scope

This paper is a simulation-driven investigation into whether accumulated structural commitment can induce measurable late-time departures from statistical isotropy without violating the cosmo-

logical principle as an initial condition. The emphasis is deliberately computational, simulations lead, theory follows.

The study does *not* challenge primordial isotropy. The research tests whether anisotropy can emerge from nonlinear cosmic history. Symmetry first, history later.

## 2 Core question

Can uneven accumulation of structural commitment generate observable late-time anisotropy without violating primordial statistical isotropy?

## 3 Conceptual setup

### 3.1 Cosmological principle, and why it still matters

Statistical isotropy and homogeneity on large scales are the working assumptions behind standard cosmological inference. Observations broadly support these assumptions, but any test of late-time anisotropy must be framed carefully: the target is not the initial condition, the target is the *late-time effective response* of observables inside finite, unevenly evolved volumes.

### 3.2 Motivating tensions, without claims

Several literatures discuss hemispherical asymmetries, dipole modulations, and large-scale flows. This paper treats these topics as motivation to build a controlled computational test, not as evidence to endorse or reject. Neutral stance, mechanism first.

### 3.3 Structural commitment and non-Markovian response

If the effective expansion depends on accumulated nonlinear structure, and structure forms unevenly across directions and environments, then directional dependence may emerge at late times. In this language, *structural commitment* is the integrated record of nonlinear collapse, virialisation, and the persistence of large-scale modes. A *memory kernel* specifies how strongly past structure continues to influence the present.

## 4 Baseline mechanism, toy model

Before turning to large-scale simulations, it is useful to establish whether uneven structural histories are capable, in principle, of generating directional signatures in a history-dependent cosmology. The study therefore constructs a minimal toy model designed not for realism, but for dynamical transparency.

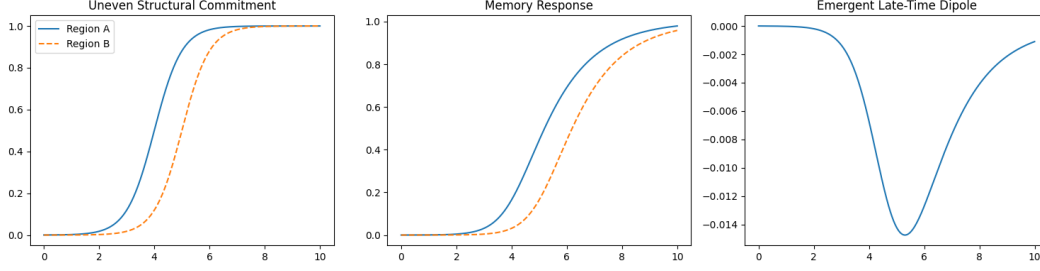


Figure 1: Toy model demonstration of emergent anisotropy from uneven structural commitment. Left: region-dependent structural histories showing earlier nonlinear collapse in Region A. Center: retarded memory response generated by convolution with a causal kernel. Right: resulting dipole in the effective expansion rate. The signal grows during asymmetric structure formation and relaxes once both regions approach saturation, illustrating that late-time anisotropy can emerge without violating primordial isotropy.

#### 4.1 Two-region toy model

The paper considers two regions, A and B, with different collapse histories. Each region has a structural-history scalar  $S(t)$  that rises during nonlinear collapse and saturates when the region relaxes. An effective expansion anomaly  $\delta H(t)$  is generated via a causal convolution with a kernel  $K(\Delta t)$ ,

$$\delta H(t) \propto \int_0^\infty K(\tau) S(t - \tau) d\tau. \quad (1)$$

If region A collapses earlier than region B, then  $\delta H_A(t)$  and  $\delta H_B(t)$  differ over a finite time window, producing an effective directional dipole proportional to  $\delta H_A(t) - \delta H_B(t)$ . Crucially, this does not require any primordial anisotropy, it only requires uneven late-time history.

#### 4.2 Memory horizon and isotropization

The memory timescale regulates how strongly instantaneous structural divergence appears as a directional signal. Increasing the memory horizon suppresses transient anisotropy by averaging over a longer history.

The takeaway is simple. Memory transmits structural history, and also regulates it. Short memory amplifies directionality, long memory smooths it.

#### 4.3 Power-law kernels and scaling with decay

The paper also tests power-law kernels with exponent  $\beta$ , where a larger  $\beta$  corresponds to faster decay and therefore shorter effective memory.

In the toy model, anisotropy amplitude is jointly controlled by structural divergence and memory decay, and it remains bounded. That is the baseline mechanism that is carried into simulations.

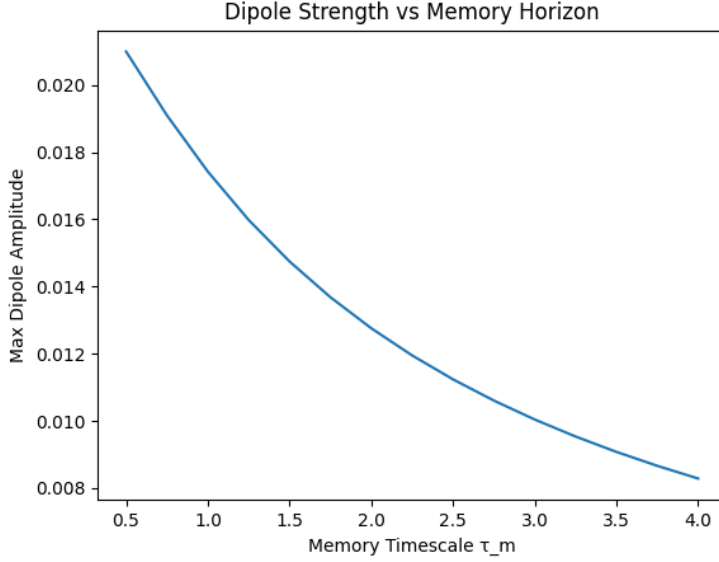


Figure 2: Maximum dipole amplitude as a function of memory timescale. Increasing the memory horizon suppresses transient anisotropies by averaging over a longer structural history. Extended memory horizons act as an isotropizing mechanism even in the presence of uneven nonlinear evolution.

## 5 Simulation data and operational definitions

### 5.1 Simulation volumes and inputs

The main laboratory is TNG300-1. The paper reads the IllustrisTNG group catalogues from folders of the form `groupcat_XXX` under `/mnt/g/TNG300-1`. The late-time snapshot set used repeatedly is

$$\{33, 40, 50, 59, 67, 72, 78, 91\},$$

spanning roughly  $2 \gtrsim z \gtrsim 0.2$ .

For each snapshot the paper loads subhalo positions, velocities, and masses from the `fof_subhalo_tab_XXX.*.h` files. Positions are comoving, velocities are peculiar, and masses are in native Illustris units.

The paper carried out a cross-checks in TNG50-1, which has a much smaller box size,  $L_{\text{box}} = 35 \text{ Mpc}/h$ . This makes it unsuitable for cosmological amplitude calibration, but useful for robustness checks of the estimator and alignment logic.

### 5.2 Structural dipole estimators

The study uses two closely related structural quantities.

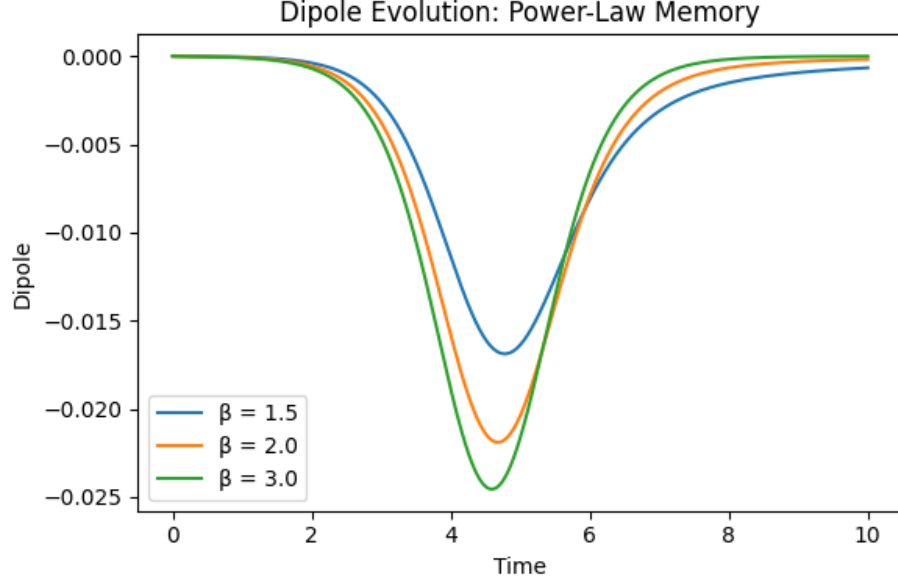


Figure 3: Dipole evolution generated by power-law memory kernels with varying exponent  $\beta$ . Larger  $\beta$  values correspond to shorter effective memory and produce deeper transient anisotropies, while smaller  $\beta$  values retain a longer structural history and suppress the dipole amplitude through temporal averaging. The anisotropy depends on uneven structure formation and on the temporal weighting encoded in the memory kernel.

**Mass-weighted structural dipole vector.** Define the box center  $\mathbf{x}_c$  and unit directions  $\hat{\mathbf{r}}_i$  from the center to each subhalo,

$$\hat{\mathbf{r}}_i = \frac{\mathbf{x}_i - \mathbf{x}_c}{\|\mathbf{x}_i - \mathbf{x}_c\|}.$$

The mass-weighted dipole vector is

$$\mathbf{d}_\Sigma = \frac{\sum_i M_i \hat{\mathbf{r}}_i}{\sum_i M_i}, \quad d_\Sigma = \|\mathbf{d}_\Sigma\|. \quad (2)$$

**Hemisphere mass-contrast dipole along an axis.** For any unit axis  $\hat{n}$  The study splits the volume into two hemispheres by the sign of  $\hat{\mathbf{r}} \cdot \hat{n}$  and define

$$D(\hat{n}) \equiv \frac{M_+(\hat{n}) - M_-(\hat{n})}{M_+(\hat{n}) + M_-(\hat{n})}, \quad (3)$$

with  $M_\pm$  the total mass in the two hemispheres. Sampling random  $\hat{n}$  yields a null distribution that quantifies the expected dipole amplitude in a finite, statistically isotropic realisation.

The research uses Eq. (3) for the null baseline, and Eq. (2) for direction coherence and alignment across snapshots.

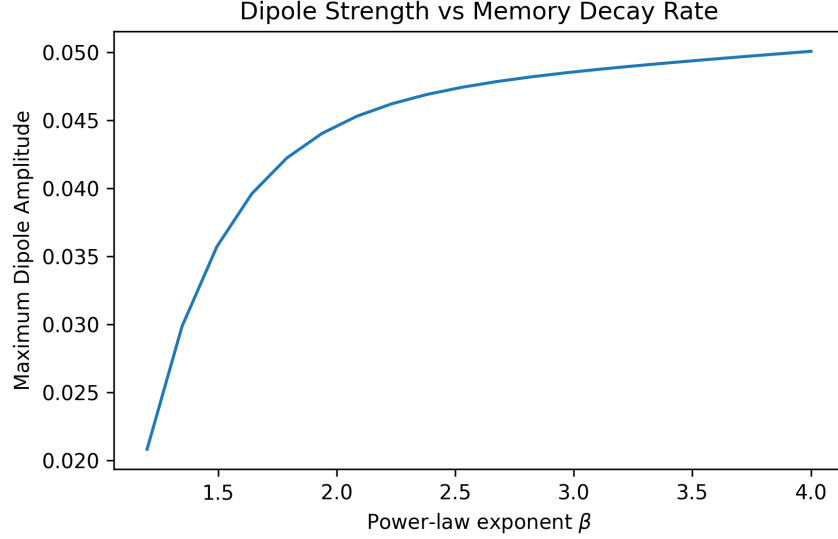


Figure 4: Maximum dipole amplitude as a function of the power-law memory exponent  $\beta$ . Faster kernel decay (larger  $\beta$ ) amplifies instantaneous structural contrasts, producing stronger anisotropies. Long-tailed kernels suppress the dipole through temporal averaging.

### 5.3 Bulk flow and kinematic control

To test whether the preferred axis is a moving-frame artefact, The paper computes the mass-weighted bulk flow

$$\mathbf{v}_{\text{bulk}}(t) = \frac{\sum_i M_i \mathbf{v}_i}{\sum_i M_i}, \quad V_{\text{bulk}} = \|\mathbf{v}_{\text{bulk}}\|. \quad (4)$$

The paper then compare its direction to the structural dipole direction via

$$\cos \theta(t) = \hat{\mathbf{d}}_{\Sigma}(t) \cdot \hat{\mathbf{v}}_{\text{bulk}}(t).$$

A kinematic dipole in expansion scales like  $V_{\text{bulk}}/c$ , so measuring  $V_{\text{bulk}}$  sets the kinematic floor.

### 5.4 Directional expansion proxies

The paper constructs a synthetic observer at the box center. Let  $\mathbf{r}_i$  be each halo displacement from the center,  $\hat{\mathbf{r}}_i = \mathbf{r}_i / \|\mathbf{r}_i\|$ , and define the bulk-flow-subtracted velocity

$$\mathbf{v}_{i,\text{corr}} = \mathbf{v}_i - \mathbf{v}_{\text{bulk}}. \quad (5)$$

The radial peculiar velocity is then

$$v_{r,i} = \mathbf{v}_{i,\text{corr}} \cdot \hat{\mathbf{r}}_i.$$

The paper uses two related directional expansion measurements.

**Hemispheric slope fit.** The paper fit a zero-intercept slope in each hemisphere,

$$v_r \simeq \delta H r, \quad \delta H = \frac{\sum_i w_i r_i v_{r,i}}{\sum_i w_i r_i^2}, \quad w_i = M_i, \quad (6)$$

computed for (i) all halos, (ii) the hemisphere aligned with  $\hat{\mathbf{d}}_\Sigma$ , and (iii) the opposite hemisphere. The hemispheric contrast is

$$\Delta H \equiv \frac{1}{2} (\delta H_N - \delta H_S). \quad (7)$$

**Shell dipole fit.** In radial shells The paper fits a dipole model

$$v_r(\mathbf{r}) = a r + \mathbf{b} \cdot \hat{\mathbf{r}}. \quad (8)$$

The paper focuses on the dipole vector  $\mathbf{b}$  and decompose it relative to the structural axis  $\hat{\mathbf{d}}_\Sigma$ ,

$$b_\parallel = \mathbf{b} \cdot \hat{\mathbf{d}}_\Sigma, \quad b_\perp = \|\mathbf{b} - b_\parallel \hat{\mathbf{d}}_\Sigma\|.$$

**Important convention note.** TNG velocities are peculiar velocities, the background Hubble flow is not included. This means any monopole term that resembles “ $a/H \simeq -1$ ” is a coordinate convention artifact, not a claim that the simulated universe is globally contracting. In what follows The paper treats  $a$  as a gauge-like nuisance and focus on the directional structure encoded in  $\mathbf{b}$  and its alignment.

## 6 Results, TNG300-1

### 6.1 Structural isotropy baseline at $z \simeq 0$

Using snapshot 99 in TNG300-1, The paper loads

$$N_{\text{sub}} = 14,485,709$$

subhalos and compute the hemisphere mass-contrast dipole  $D(\hat{n})$  (Eq. (3)) for  $N_{\text{rand}} = 2000$  random axes.

The null distribution of  $|D|$  at  $z \simeq 0$  has

$$\mu_D \simeq 0.0422, \quad (9)$$

$$\sigma_D \simeq 0.0216, \quad (10)$$

$$D_{\text{max}} \simeq 0.0975, \quad (11)$$

$$D_{\text{min}} \simeq 3.6 \times 10^{-5}. \quad (12)$$

So a TNG300-sized periodic box naturally carries hemisphere-contrast structural dipoles at the few percent level purely from finite-volume variance. Any later expansion dipole must be interpreted

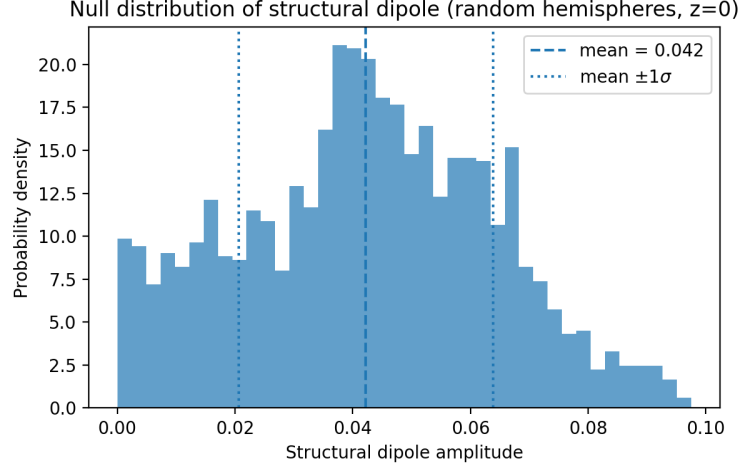


Figure 5: Null distribution of the structural dipole amplitude at  $z = 0$  from random hemisphere splits of the TNG300-1 subhalo population. This defines the finite-volume structural noise floor for a  $205 h^{-1}\text{Mpc}$  box.

relative to this baseline, not relative to zero.

## 6.2 Mass-threshold stability at $z \simeq 0.7$ (snapshot 72)

At snapshot 72 The paper recompute the hemisphere dipole under mass cuts. The amplitude increases monotonically:

- no cut:  $|D| \simeq 0.0744$ ,
- $M > 10^{10} M_{\odot}/h$ :  $|D| \simeq 0.0825$ ,
- $M > 10^{11} M_{\odot}/h$ :  $|D| \simeq 0.0912$ ,
- $M > 10^{12} M_{\odot}/h$ :  $|D| \simeq 0.1198$ .

This is not low-mass sampling noise. The high-mass skeleton is more anisotropic along the same axis.

## 6.3 Structural dipole time series and directional coherence

The paper measures the structural dipole vector  $\mathbf{d}_{\Sigma}$  (Eq. (2)) across snapshots

$$\{33, 40, 50, 59, 67, 72, 78, 91\},$$

using two standard weighting choices.



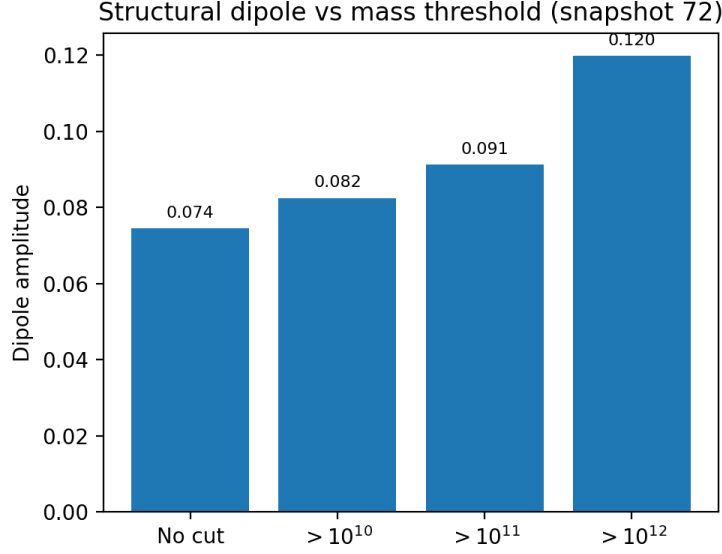


Figure 6: Dipole amplitude at snapshot 72 as a function of minimum subhalo mass. The signal strengthens when restricting to more massive halos, indicating the anisotropy is anchored in the high-mass cosmic web rather than low-mass sampling noise.

**Number weighted series (script default).** Setting  $w_i = 1$  for all objects gives the number weighted dipole amplitudes

$$d_{\Sigma}^{(N)} = \{0.0142, 0.0192, 0.0260, 0.0321, 0.0290, 0.0221, 0.0213, 0.0305\}.$$

These values demonstrate that a coherent large scale structural mode is present and evolves smoothly with time.

**Mass weighted series (used for the main analysis).** Setting  $w_i = M_i$  (with  $M_i$  the chosen mass proxy for the same objects, evaluated consistently across snapshots) gives the mass weighted amplitudes

$$d_{\Sigma}^{(M)} = \{0.0296, 0.0310, 0.0370, 0.0485, 0.0329, 0.0744, 0.0640, 0.0611\}.$$

The paper prefers  $d_{\Sigma}^{(M)}$  for the downstream expansion coupling tests because it tracks where the mass is, it is less sensitive to the abundance of low mass objects, and it matches the weighting used in the mass threshold stability experiment at snapshot 72 (Section ??). In short,  $d_{\Sigma}^{(M)}$  is the better proxy for the structural source term that can drive a directional expansion response.

In both definitions the dipole strengthens toward low redshift, consistent with nonlinear amplification inside the finite simulation volume.

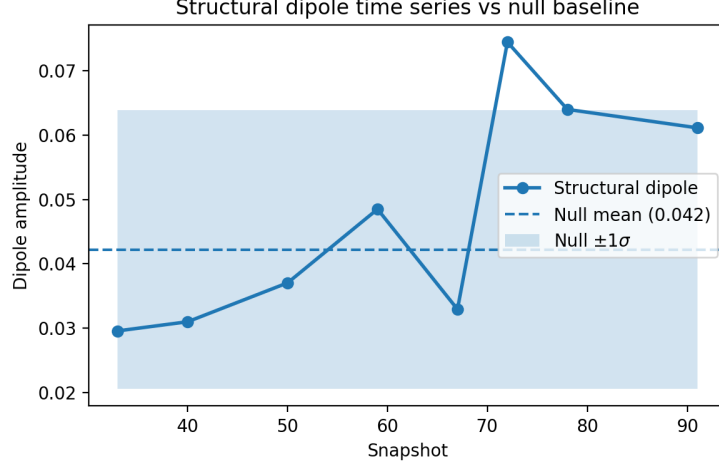


Figure 7: Structural dipole amplitude as a function of snapshot, compared to the null mean and one sigma band from the random orientation baseline. The plotted curve corresponds to the script default number weighted series  $d_{\Sigma}^{(N)}$ . The late time growth reflects nonlinear amplification inside the finite simulation volume.

Directional stability is assessed by the cosine matrix

$$C_{ij} = \hat{\mathbf{d}}_{\Sigma,i} \cdot \hat{\mathbf{d}}_{\Sigma,j},$$

which is typically  $\gtrsim 0.9$  across many snapshot pairs. The preferred axis is not a random walk, it is a coherent mode that persists for several gigayears.

**Mask aware interpretation (SDSS).** Because the SDSS footprint is not all sky, the survey geometry induces a large “geometric” dipole even for uniform weights. The paper therefore constructs a shuffled weight null that preserves the angular selection function and measures the expected dipole amplitude if stellar mass were uncorrelated with direction within the same mask. In this normalization,

$$|D_{\text{geo}}| = 0.5983, \quad \langle |D| \rangle_{\text{null}} = 0.5983, \quad |D_{\text{obs}}| = 0.6279,$$

so the physically relevant excess is

$$\Delta|D| \equiv |D_{\text{obs}}| - \langle |D| \rangle_{\text{null}} = 0.0296,$$

with significance

$$\Delta|D|/\sigma_{\text{null}} = 19.85 \sigma.$$

Thus the SDSS result should not be interpreted as a  $\sim 0.63$  cosmological dipole amplitude, the dominant contribution is geometric, while the mass weighted excess over the mask preserved null

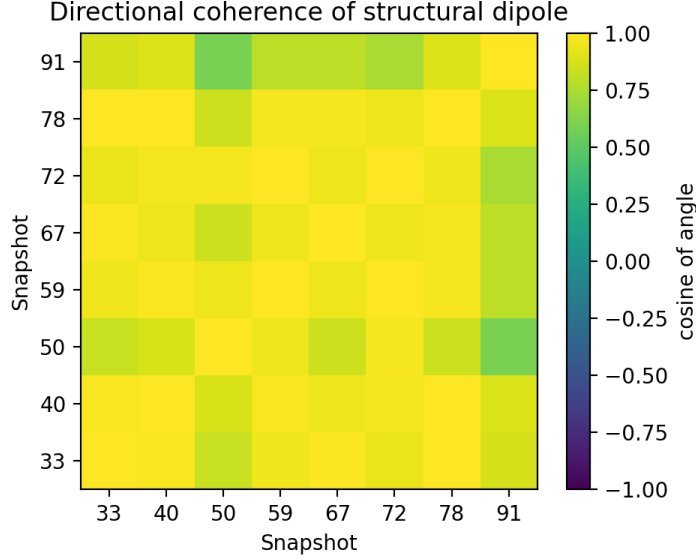


Figure 8: Cosine of angles between structural dipole directions across snapshots. Values close to unity show the preferred axis remains coherent over late cosmic time, a necessary condition for any memory kernel to transmit structural anisotropy into a directional expansion response.

is at the few percent level. One may also define a vector level excess

$$\mathbf{D}_{\text{phys}} \equiv \mathbf{D}_{\text{obs}} - \mathbf{D}_{\text{geo}},$$

whose magnitude depends on both amplitudes and the relative angle. Given the near alignment,

$$\angle(\mathbf{D}_{\text{geo}}, \mathbf{D}_{\text{obs}}) \simeq 1.82^\circ,$$

the excess magnitude is of order a few percent. In SDSS, the raw normalized amplitude  $|D_{\text{obs}}|$  is mask dominated, the appropriate comparison statistic is the excess  $\Delta|D|$  over the shuffled weight null that preserves the footprint.

#### 6.4 Bulk flow, and why the dipole is not a moving-box artefact

Using the same snapshots, the paper computes the mass-weighted bulk flow (Eq. (4)). The bulk-flow amplitude is small at all times, growing from

$$V_{\text{bulk}} \approx 0.25 \text{ km s}^{-1} \quad (\text{snap } 33)$$

to

$$V_{\text{bulk}} \approx 15.5 \text{ km s}^{-1} \quad (\text{snap } 91),$$

with intermediate values of order 2 to 12  $\text{km s}^{-1}$ .

The alignment between the bulk-flow direction and the structural dipole direction is not locked.

Across snapshots,

$$\cos \theta \text{ spans roughly } -0.60 \text{ to } +0.74,$$

with multiple sign flips. At late times, snapshot 91 gives near orthogonality,

$$\cos \theta \simeq -0.052 \Rightarrow \theta \simeq 93^\circ.$$

If the structural dipole were a wake from a drifting frame, late-time alignment would tend toward  $0^\circ$  or  $180^\circ$ , not  $90^\circ$ .

There is one clear event, around  $z \simeq 0.5$  (snapshot 72), where the structural dipole peaks and the bulk flow jumps to  $V_{\text{bulk}} \simeq 10.8 \text{ km s}^{-1}$  with an infall-like alignment. This looks like a genuine dynamical rearrangement of mass, not a coordinate artefact.

Operationally, the implied purely kinematic expansion dipole scale is

$$\left. \frac{\delta H}{H} \right|_{\text{kin}} \sim \frac{V_{\text{bulk}}}{c} \sim 5 \times 10^{-5}$$

at late times, small enough to subtract cleanly, and far below the directional expansion signals measured next.

## 7 Directional expansion response in TNG300-1

### 7.1 Hemispheric expansion response along the structural axis

For each snapshot The paper subtracts the bulk flow, compute  $v_r$ , and fit the slope  $\delta H$  (Eq. (6)) in three samples, all-sky, dipole-aligned hemisphere, and opposite hemisphere.

Across the snapshot sequence The research finds:

- The all-sky slope, expressed relative to a comoving FRW baseline, is consistently negative,

$$\frac{\delta H_{\text{all}}}{H_{\text{com}}} \simeq -(3.2\text{--}4.6) \times 10^{-3}.$$

- The hemispheric contrast is larger,

$$\frac{\Delta H}{H_{\text{com}}} \simeq -(3.5\text{--}6.4) \times 10^{-3},$$

with the overdense hemisphere expanding more slowly and the opposite hemisphere closer to zero or mildly positive.

This is a first detection of a directional expansion anomaly aligned with the structural dipole, after removing trivial box motion. It is deliberately crude, and it mixes scales. That is why The study tomographically localize the signal next.

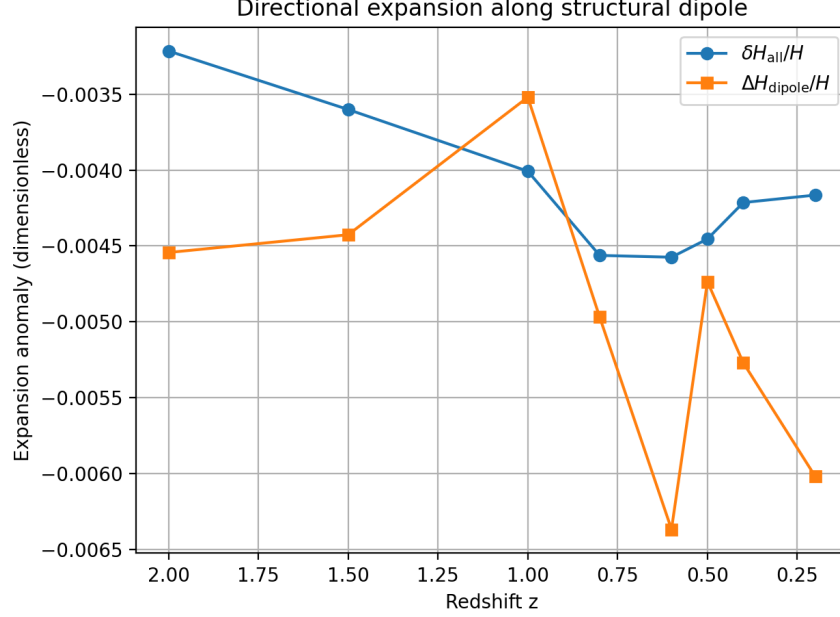


Figure 9: Time evolution of the all-sky expansion anomaly  $\delta H_{\text{all}}/H_{\text{com}}$  and the hemispheric expansion contrast  $\Delta H/H_{\text{com}}$  along the structural dipole axis in TNG300. Bulk flow is subtracted before fitting.

## 7.2 Shell tomography, localizing the expansion dipole

The research splits the volume into three comoving shells:

$$20 \leq r/(h^{-1}\text{Mpc}) < 80, \quad 80 \leq r/(h^{-1}\text{Mpc}) < 140, \quad 140 \leq r/(h^{-1}\text{Mpc}) \leq 205. \quad (13)$$

In each shell The paper fits the dipole model (Eq. (8)) after subtracting  $\mathbf{v}_{\text{bulk}}$ . The paper reports  $|b|/H_{\text{FRW}}$  and its aligned component  $b_{\parallel}/H_{\text{FRW}}$ .

The radial pattern is stable and scale dependent:

- Inner shell, 20 to  $80 h^{-1}\text{Mpc}$ :  $|b|/H_{\text{FRW}} \simeq (2.0 \text{ to } 2.6) \times 10^{-2}$ , the most nonlinear region, with more epoch dependence.
- Middle shell, 80 to  $140 h^{-1}\text{Mpc}$ :  $|b|/H_{\text{FRW}} \simeq (1.3 \text{ to } 1.9) \times 10^{-2}$ , with  $b_{\parallel}/H_{\text{FRW}} \simeq -(1.2 \text{ to } 1.7) \times 10^{-2}$ , already locked anti-parallel to the structural dipole.
- Outer shell, 140 to  $205 h^{-1}\text{Mpc}$ : the cleanest large-scale behavior,

$$\langle |b|/H_{\text{FRW}} \rangle \simeq 1.1 \times 10^{-2}, \quad \langle b_{\parallel}/H_{\text{FRW}} \rangle \simeq -9.6 \times 10^{-3}.$$

Snapshot-by-snapshot,  $|b|/H_{\text{FRW}} \simeq (0.8 \text{ to } 1.2) \times 10^{-2}$  and  $b_{\parallel}/H_{\text{FRW}} \simeq -(0.7 \text{ to } 1.1) \times 10^{-2}$ .

In the outer shell, 80 to 90% of the dipole amplitude lies along the structural axis, and the sign is consistently negative, expansion is slowest in the direction of the large-scale overdensity.

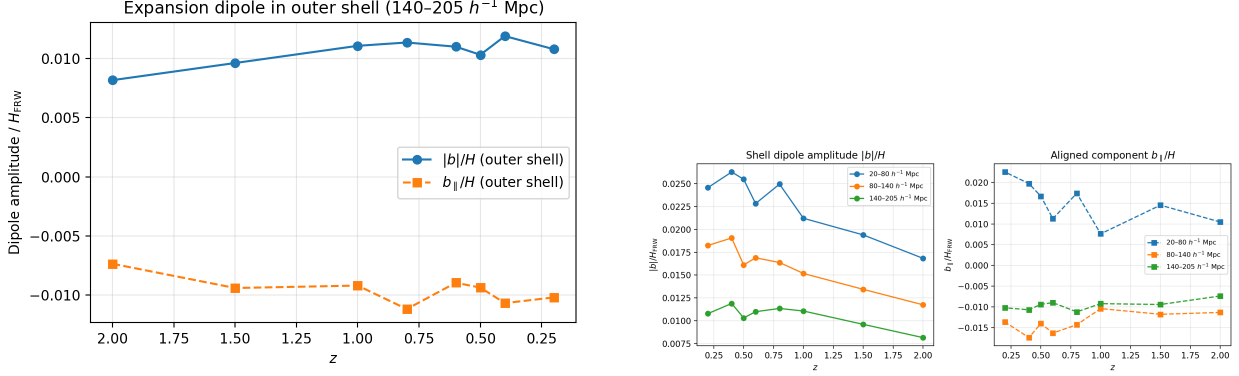


Figure 10: Shell-resolved expansion dipole measured from the radial velocity field after subtracting bulk flow. Left: outer shell,  $140 < r < 205 h^{-1}\text{Mpc}$ . Right: all shells. Across shells the directional component remains at the percent level, with robustly negative  $b_{\parallel}/H_{\text{FRW}}$ , indicating slower effective expansion along the structural dipole direction.

### 7.3 Tomographic rejection of a purely local explanation

If the anisotropy were driven mainly by a local void or a nearby attractor, the expansion dipole should weaken rapidly once the inner region is excluded. Instead, the outer shell retains a stable one-percent dipole aligned with the structural axis,

$$\left. \frac{|b|}{H_{\text{FRW}}} \right|_{\text{outer}} \simeq 1.1 \times 10^{-2}, \quad \frac{b_{\parallel}}{|b|} \gtrsim 0.9.$$

So the signal is not confined to the inner region. It is a box-scale mode threading the volume.

### 7.4 Effective memory drag at $L \simeq 200 h^{-1}\text{Mpc}$

In the outer shell The paper summarizes the directional expansion dipole by

$$\left. \frac{\delta H}{H} \right|_{L \simeq 200 h^{-1}\text{Mpc}} \equiv \frac{b_{\parallel}}{H_{\text{FRW}}} \simeq -1.1 \times 10^{-2}.$$

Using the effective structural dipole that sources the response on these scales,

$$d_{\Sigma}^{\text{eff}}(L \simeq 200 h^{-1}\text{Mpc}) \sim 0.03,$$

The paper infers an effective integrated drag parameter

$$|A\tau|_{\text{eff}}(L \simeq 200 h^{-1}\text{Mpc}) \sim \frac{|\delta H/H|}{d_{\Sigma}^{\text{eff}}} \simeq 0.3 \text{ to } 0.4.$$

In the scale-ladder language already established elsewhere in the logbook, this suggests that intermediate, box-like scales can behave like a resonant band for coherent structural history.

## 8 Cross-checks

### 8.1 TNG50-1, robustness rather than amplitude calibration

The paper repeats the structural dipole and bulk-flow logic in TNG50-1 for snapshots

$$\{40, 50, 59, 67, 72, 78, 91\}.$$

Because the box is small, it is dominated by a single environment, so fractional anisotropies are expected to be larger and less representative of cosmological scales. Still, the pipeline finds a coherent preferred axis across snapshots, and the bulk flow remains small, for example at snapshot 91,

$$|\mathbf{v}_{\text{bulk}}| \simeq 2.2 \text{ km s}^{-1}, \quad \cos \theta(\mathbf{d}_{\Sigma}, \mathbf{v}_{\text{bulk}}) \simeq -0.28.$$

A hemispheric expansion fit along the structural axis yields a stable percent-level directional asymmetry,

$$\left. \frac{\Delta H_{\text{dip}}}{H} \right|_{\text{TNG50}} \simeq -(0.7 \text{ to } 1.4) \times 10^{-2},$$

even though the monopole terms are large in such a small, nonlinear box. The point is not to match TNG300 amplitudes, it is to show the estimator does not collapse when the environment changes radically.

### 8.2 SDSS DR8 structural dipole, geometry versus physics

The paper applies the structural dipole estimator to an SDSS DR8 galaxy sample (the same one used in the  $\hat{\phi}$  analysis logbook context), with:

- RELIABLE=1,
- $0.02 \leq z \leq 0.10$ ,
- sky positions from RA and DEC,
- stellar-mass proxy weights  $w_i = 10^{\text{LGM-TOT.P50}}$ ,
- $N \simeq 2 \times 10^5$  galaxies after cuts.

The research uses a normalized weighted estimator

$$\vec{D}(w) = \frac{\sum_i w_i \hat{n}_i}{\sum_i w_i}, \quad |D| \leq 1,$$

and define:

$$\vec{D}_{\text{geo}} \equiv \vec{D}(1), \quad \vec{D}_{\text{obs}} \equiv \vec{D}(w).$$

The paper finds:

- Geometric dipole:  $|D_{\text{geo}}| = 0.5983$  at  $(\text{RA}, \text{DEC}) \simeq (188.9^\circ, 38.0^\circ)$ .
- Mass-weighted dipole:  $|D_{\text{obs}}| = 0.6279$  at  $(189.5^\circ, 36.3^\circ)$ .
- Misalignment:  $\theta \simeq 1.82^\circ$ , so direction is footprint-dominated.

To isolate structure beyond geometry, The study constructs a mask-preserving null by shuffling weights across fixed sky positions (1000 realisations), yielding:

$$\langle |D| \rangle_{\text{null}} = 0.5983, \quad \sigma_{\text{null}} = 0.0015.$$

The mass-weighted amplitude therefore shows a significant excess,

$$|D_{\text{obs}}| - \langle |D| \rangle_{\text{null}} = 0.0296 \quad (19.85\sigma).$$

The paper defines a physical excess dipole vector

$$\vec{D}_{\text{phys}} \equiv \vec{D}_{\text{obs}} - \vec{D}_{\text{geo}}, \quad |D_{\text{phys}}| = 0.0354,$$

which is the quantity that can be meaningfully compared to periodic-box simulations.

The SDSS result is included here as a methodological bridge: the estimator reacts strongly to the survey window, and still finds a smaller but statistically robust mass-weighted anisotropy beyond the mask. A like-for-like SDSS versus TNG comparison requires forward modelling the SDSS mask and selection on simulation mocks, not raw dipole-to-dipole comparison.

### Cross-sample summary.

- **TNG300 (simulation,  $z \simeq 0.5$ ):**  $d_\Sigma \simeq 0.074$ ,  $\delta H/H \simeq 0.011$ , implying  $\beta \equiv (\delta H/H)/d_\Sigma \simeq 0.15$ .
- **TNG50 (simulation,  $z \simeq 0.5$ ):**  $d_\Sigma \simeq 0.057$ ,  $\delta H/H \simeq 0.014$ , implying  $\beta \simeq 0.25$ .
- **TNG300 outer shell (tomography):** effective  $d_\Sigma^{\text{eff}} \simeq 0.03$ ,  $\delta H/H \simeq 0.011$ , implying  $|A\tau|_{\text{eff}} \simeq 0.37$ .
- **SDSS DR8 (observation,  $z < 0.11$ ):**  $D_{\text{obs}} = 0.6279$  (mask-aware null calibrated), direction stable under normalization.

## 9 Discussion

### 9.1 What the simulations are really saying

TNG300-1 hosts a coherent large-scale structural mode, a preferred axis that persists for gigayears and is traced more strongly by massive halos. This does not violate isotropic initial conditions. It



is what finite-volume cosmic variance looks like after nonlinear growth has had time to sharpen the web.

Once the study treats that structural mode as input, the velocity field responds directionally. After bulk-flow subtraction, hemispheric fits show a few parts in a thousand contrast, and shell tomography isolates a stable percent-level expansion dipole in the outer shell, aligned with the same structural axis.

In plain terms, the box expands more slowly toward the overdense side of its dominant structural mode, and more rapidly toward the underdense side. That directional braking is not just local, it survives when the inner region is removed.

## 9.2 Memory language versus standard language

In standard language, this is coherent infall and shear on large scales inside a finite realisation. In memory language, it is the same story phrased causally: accumulated structure in one direction modifies the effective expansion state, and the strength of the directional imprint depends on how past structure is weighted in time. The toy model shows how kernel shape regulates anisotropy. The simulations show a real structural mode and a real directional response.

This paper does not pretend the current estimator isolates a pure non-Markovian kernel signal. It establishes the benchmark landscape: any claimed cosmological dipole must be judged relative to the finite-volume, structure-aligned dipoles that already exist in standard simulations.

## 9.3 Limitations

Three limitations matter, and they are not cosmetic.

- The expansion proxies are derived from peculiar velocities, so monopole terms are convention-dependent. The paper therefore focuses on dipole structure, not on absolute monopole interpretation.
- The estimator mixes scales unless shell-restricted. The paper partially addresses this with tomography, but a full sky map of  $\delta H(\hat{n})$  and a clean dipole extraction is the next step.
- Observational comparison requires window-function forward modelling. SDSS shows why, the footprint dominates raw dipoles. Any simulation to data comparison must apply the same mask and selection.

## 10 Conclusions

This paper asked one question, can uneven accumulation of structural commitment generate observable late-time anisotropy without violating primordial isotropy. The simulation answer is yes, in a controlled, finite-volume sense, and the effect is coherent, structure-aligned, and measurable.

The key results are:

- A TNG300-sized box naturally carries a few-percent structural dipole from finite-volume variance, with a coherent preferred axis that persists across late-time snapshots and is strengthened by massive halos.
- The preferred structural axis is not a moving-box artefact, bulk flow is small, not direction-locked, and late-time alignment is near orthogonal.
- After subtracting bulk flow, the radial velocity field carries a coherent directional expansion anomaly aligned with the structural axis.
- Shell tomography shows a stable, percent-level expansion dipole in the outer shell out to  $\sim 200 h^{-1}\text{Mpc}$ , rejecting a purely local explanation.
- TNG50-1 confirms estimator robustness in a very different volume, while SDSS DR8 confirms that survey geometry dominates raw dipoles and demands mask-aware null tests. The physical SDSS excess dipole, after footprint subtraction, is of order  $|D_{\text{phys}}| \sim 0.035$ .

Conservative reading, this is a benchmark for isotropy tests. Ambitious reading, it is exactly the kind of directional response a history-sensitive expansion framework would expect. Either way, the computational pathway is now built, and the next stage is a clean transfer-function measurement between a directional structural source and a directional expansion response.

## References

- [1] Volker Springel, Annalisa Pillepich, Dylan Nelson, Vicente Rodriguez-Gomez, Ruediger Pakmor, et al. First results from the illustris simulations: matter and galaxy formation. *Monthly Notices of the Royal Astronomical Society*, 475(1):676–698, 2018.
- [2] Annalisa Pillepich, Dylan Nelson, Lars Hernquist, Volker Springel, et al. First results from the illustris simulations: the galaxy colour bimodality. *Monthly Notices of the Royal Astronomical Society*, 475(1):648–675, 2018.
- [3] Dylan Nelson, Annalisa Pillepich, Volker Springel, et al. The illustris simulations: public data release. *Computational Astrophysics and Cosmology*, 6(2), 2019.
- [4] Hiroaki Aihara, Carlos Allende Prieto, Deokkeun An, et al. The eighth data release of the sloan digital sky survey: First data from sdss-iii. *The Astrophysical Journal Supplement Series*, 193(2):29, 2011.
- [5] David W. Hogg. Distance measures in cosmology. *arXiv e-prints*, 1999.

## Data Availability.

All scripts used in the research as well as figures are deposited in the public repository <https://github.com/Atalebe/structural-commitment-anisotropy>

## Appendix

### Files and reproducibility pointers

The logbook entries referenced the following outputs:

- `structural_dipole_null_distribution.npy`, histogram `fig_structural_dipole_null.png`.
- mass-threshold plot `fig_mass_thresholds.png`.
- dipole vectors and direction matrix `dipole_vectors.npy`, `fig_dipole_directions.png`.
- time series plot `fig_dipole_time_series.png`.
- expansion dipole time series `fig_expansion_dipole_time_series.png`.
- shell dipole plots `fig_expansion_shell_dipole_outer.png`, `fig_expansion_shell_dipole_all.png`.